

# Density Profile of a Cool Core of Galaxy Clusters

Naomi Ota,<sup>1</sup> Kiyokazu ONZUKA,<sup>2</sup> and Kuniaki MASAI<sup>2</sup>

<sup>1</sup>*Department of Physics, Nara Women's University, Kitaoyanishi-machi, Nara, Nara 630-8506*  
*naomi@cc.nara-wu.ac.jp*

<sup>2</sup>*Department of Physics, Tokyo Metropolitan University, 1-1 Minami-Osawa, Hachioji, Tokyo 192-0397*

(Received ; accepted )

## Abstract

The density profile of a cool core of intracluster gas is investigated for a cluster of galaxies that is initially in the virial equilibrium state, and then undergoes radiative cooling. The initial gas profile is derived under the assumption that the gas is hydrostatic within the dark-matter potential presented by the “NFW” or King model, and has a polytropic profile. The contribution of masses of gas and galaxies to the potential in the calculation is ignored compared to the dark matter. The temperature and density profiles of gas in its quasi-hydrostatic cooling phase, which is expected to last for  $\sim$ Gyr, is then calculated for different initial gas profiles. It is found that in the quasi-hydrostatic cooling phase, while the temperature decreases to about one-third, the density increases by a factor of 4–6 at the cluster center in comparison with their initial polytropic values, though the profiles over the core depend on the dark-matter potential. Hence, the core radius in the quasi-hydrostatic cooling gas appears to be smaller than that in the initial polytropic gas. We compared the density profile of the cool core with observations to find that, while the initial density is around the upper bounds of large-core ( $> 100$  kpc) clusters, most likely relaxed, but the cooling is not yet significant, the central density under quasi-hydrostatic cooling falls between the mid- and high-values of small ( $< 100$  kpc)- or cool-core clusters. It is also found for the quasi-hydrostatic cooling gas that the entropy profile roughly agrees with the best-fit model to the ACCEPT cluster sample with a low central entropy; also, the pressure gradient in the inner core is close to that of the REXCESS sample. X-ray surface brightness calculated for the quasi-hydrostatic cooling gas is well represented by the conventional double  $\beta$ -model, giving a physical basis for applying the double  $\beta$ -model to cool-core clusters.

**Key words:** galaxies: clusters: general – galaxies: cooling flows – galaxies: intergalactic medium – X-rays: galaxies: clusters

## 1. Introduction

Clusters of galaxies offer excellent laboratories for the thermal evolution of cosmic baryons; the objects are filled with hot ( $T \sim 10^7 - 10^8$  K), highly ionized intracluster gas, and the baryon fraction in massive clusters is close to the cosmic value. Since the time scale of radiative cooling at the center of regular clusters is estimated to be shorter than the Hubble time, their core regions are thought to be affected by cooling. According to statistical studies of clusters using X-ray observations, the proportion of clusters having a compact, cool core (often termed CC clusters) is roughly 50% (e.g., O'Hara et al. 2006; Ota et al. 2006; Chen et al. 2007; Santos et al. 2008; Cavagnolo et al. 2009; Hudson et al. 2010).

Based on earlier works on the peaked surface brightness that cooling core clusters exhibit, it was suggested that the global cooling-flow would occur unless some heating process balances with radiative cooling (e.g., Fabian 1994). The similarity and smoothness in cooling profiles indicate the need for continuous, distributed heat source (for review, e.g., Peterson & Fabian 2006). On the other hand, a possible mild inflow with a quasi-hydrostatic balance is proposed to account for the observed temperature profiles of cooling cores (Masai & Kitayama 2004). Later, using

a hydrodynamics code, Akahori & Masai (2006) demonstrate that such a cooling phase lasts for  $\sim$  Gyr, and then breaks down into global cooling-flow. They discuss the origin of the observed two-peaked core-size distribution (Ota & Mitsuda 2002; Ota & Mitsuda 2004) in view of the thermal evolution.

While the intracluster gas has often been studied on the basis of the conventional isothermal  $\beta$ -model, a deviation therefrom has been commonly observed at the center of cooling-core clusters; they exhibit a systematically higher central density, while their profiles are fairly universal outside  $0.1r_{500} \sim 100$  kpc (e.g., Neumann & Arnaud 1999). To better reproduce those X-ray observations, some authors have introduced empirical models, such as a double  $\beta$ -model (e.g., Jones & Forman 1984), and a modified  $\beta$ -model with a cool density cusp at the center and steepening at a large radius (Vikhlinin et al. 2006). This model was well fitted to the high-resolution *Chandra* data including the core emission (see also Bulbul et al. 2010). Although those models are given in analytic forms, and therefore are simply utilized for observational studies, the physical background that they are based on is not always clear.

In the present paper, we intend to obtain a fiducial-density profile of cooling gas under quasi-hydrostatic bal-

ance. Masai & Kitayama (2004) give a temperature profile for the *initially* isothermal gas, but no density profile. We calculate the temperature of cooling gas in the same manner, but more generally consider that the gas is initially hydrostatic with an polytropic profile in the NFW (Navarro et al. 1997) or King dark matter potential. In section 2, the calculation of our model is described, and pressure and entropy as well as density of quasi-hydrostatic cooling gas are presented. In section 3, we compare those calculated quantities with observations, and also examine the application of the widely used  $\beta$ -model to X-ray surface brightness calculated for quasi-hydrostatic cooling gas. We then discuss implications on the intracluster medium (ICM) thermal evolution in the cluster core regions. Since the profiles of gas density etc. of cool cores are of interest to us, we present the quantities normalized by their central values unless specified otherwise.

## 2. Calculations

### 2.1. Initial Hydrostatic Gas Distribution

We consider a spherically symmetric galaxy cluster initially in the virial equilibrium. We ignore the mass of the gas and galaxies compared to the dark matter, which is thought to occupy typically more than 80% of the cluster mass. Thus, the gas distributes so that its pressure balances with the local gravitational potential formed by the dark matter. For a noncool core (NCC), i.e, the initial state before the cooling becomes significant, we assume that the gas is in a hydrostatic balance,

$$\frac{1}{\rho} \frac{dP}{dr} = -\frac{d\phi}{dr} \simeq -G \frac{M_{\text{DM}}(r)}{r^2}, \quad (1)$$

where  $P$  and  $\rho$  are the gas pressure and the gas density, respectively, and  $\phi$  the gravitational potential;  $M_{\text{DM}}(r)$  is the dark-matter mass contained in a radius  $r$ . We solve equation (1) with an equation of state as  $P \propto \rho^\gamma$  to obtain the initial-gas distribution, where  $\gamma = 1 + (1/N)$  for the polytrope index  $N$ . We consider the NFW distribution and the approximated King distribution (referred to as King distribution hereafter) for the dark-matter potential as shown in figure 1.

The gas-temperature profile thus obtained for the NFW potential can be expressed in the form

$$\frac{T(r^*)}{T(0)} = 1 - \frac{\gamma-1}{\gamma} \frac{U_G}{kT(0)} \left[ 1 - \frac{\log(1+r^*)}{r^*} \right] \quad (2)$$

with

$$r^* = \frac{r}{r_s} \quad \text{and} \quad U_G = \frac{\mu m G}{r_s} 4\pi r_s^3 \delta_c \rho_c, \quad (3)$$

where  $r_s$  is the characteristic radius of the NFW distribution, expressed as

$$\rho_{\text{DM}}(r^*) = \frac{\delta_c \rho_c}{r^*(1+r^*)^2}, \quad (4)$$

and  $\delta_c \rho_c$  is a constant related to the dark-matter mass,  $M_{\text{DM}}$ , through

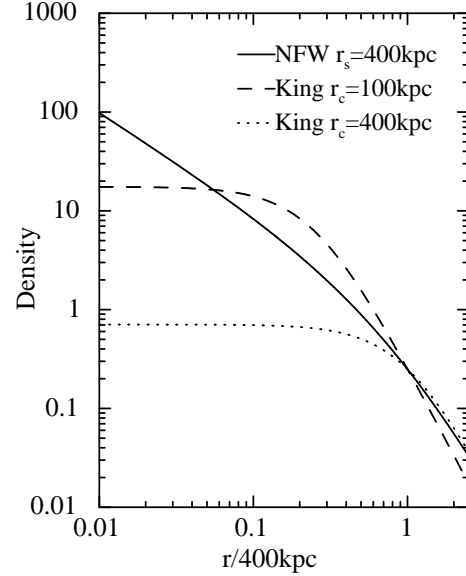


**Fig. 1.** Dark-matter density profiles with  $r_s = 400$  kpc for the NFW (solid) and  $r_c = 100$  kpc for the King (broken) distribution taken into consideration here (see text). The King profile with  $r_c = 400$  kpc is also shown for reference. The three curves are normalized so as to pass the same point at  $r = 400$  kpc.

$$M_{\text{DM}}(r^*) = 4\pi r_s^3 \delta_c \rho_c \left[ \log(1+r^*) + \frac{1}{1+r^*} - 1 \right]. \quad (5)$$

The gas-density profile is given by

$$\frac{\rho(r^*)}{\rho(0)} = \left[ \frac{T(r^*)}{T(0)} \right]^{1/(\gamma-1)} = \left[ \frac{T(r^*)}{T(0)} \right]^N. \quad (6)$$

Similarly we express the gas temperature for the King potential as

$$\frac{T(r^*)}{T(0)} = 1 - \frac{\gamma-1}{\gamma} \frac{U_G}{kT(0)} \left[ 1 - \frac{\log(r^* + \sqrt{r^{*2} + 1})}{r^*} \right] \quad (7)$$

with

$$r^* = \frac{r}{r_c} \quad \text{and} \quad U_G = \frac{\mu m G}{r_c} 4\pi r_c^3 \rho_0. \quad (8)$$

Here,  $r_c$  is the core radius of the King distribution, expressed as

$$\rho_{\text{DM}}(r^*) = \frac{\rho_0}{(1+r^{*2})^{3/2}}, \quad (9)$$

and  $\rho_0$  is the dark-matter density at the center. The dark-matter mass is given by

$$M_{\text{DM}}(r^*) = 4\pi r_c^3 \rho_0 \left[ \log(r^* + \sqrt{r^{*2} + 1}) - \frac{r^*}{\sqrt{r^{*2} + 1}} \right]. \quad (10)$$

The gas-density profile for the King potential is given by equation (6) as well.

The density profiles,  $\rho(r)/\rho(0)$ , calculated from the above equations are shown by the broken lines (denoted by NCC) in figure 2 with  $r_s = 400$  kpc for the NFW potential and with  $r_c = 100$  kpc for the King dark-matter one.

These radii are chosen for the  $\beta$ -model core radius of surface brightness ( $\propto \rho^2 T^{1/2}$ ) to be 100–200 kpc. Equations (2)–(6) are equivalent to equations (12) and (42)–(46) in Suto, Sasaki & Makino (1998), and therefore the broken lines in the left panel (NFW NCC) of figure 2 are the same as their results. We calculate the temperature profile,  $T(r)/T(0)$ , for calculations in the following subsection as well.

## 2.2. Quasi-Hydrostatic Gas Distribution under Radiative Cooling

Now we consider the gas distribution of a cool core (CC) that significantly undergoes radiative cooling. The gas is then no longer in hydrostatic balance, but should be described by hydrodynamics, since inflow toward the inner region where the cooling rate is higher would occur so as to compensate the pressure decrease due to radiation loss (Fabian 1994). Hence, the gas-temperature and gas-density profiles of the cluster core deviate from those polytropic profiles given in the last subsection.

In the early cooling phase, however, inflow is still mild and a quasi-hydrostatic condition is attained marginally until the initial cooling time,  $\tau_{\text{cool}}$ . Here,  $\tau_{\text{cool}}$  is defined by the density and temperature at the center of a virialized cluster before cooling and is typically  $\sim$  Gyr (Akahori & Masai 2006). We consider that the pressure decrease with radius due to radiation is compensated immediately by the gas inflow from the adjacent outer (and hotter) region, or the local-inflow rate is controlled by the local cooling rate, and thus a quasi-hydrostatic condition is attained.

The profile of the cooling-gas temperature,  $T'(r)$ , is then expressed approximately in a form (Masai & Kitayama 2004)

$$\frac{d \ln T'}{d \ln r} \simeq \frac{9}{5} \left( 1 - \frac{1}{3} \beta_T \frac{T_0}{T'} \right) \quad (11)$$

at  $0 < r \leq r_{\text{cool}}$ , when the variation of  $T(r)$  (NCC) is sufficiently small in this range; it should be noted that this equation was obtained originally for an isothermal mass distribution of the virial temperature  $T_0$ . Here,  $r_{\text{cool}}$  is a cooling-core radius in which the local-cooling time is shorter than the Hubble time, as  $t_{\text{cool}}(r) = 3kT(r)/[2\rho(r)\Lambda] < H_0^{-1}$  at  $r < r_{\text{cool}}$  and  $t_{\text{cool}}(r_{\text{cool}}) = H_0^{-1}$ , where  $\rho\Lambda$  represents the radiative-cooling rate per unit time. We assume  $\beta_T = 1$ , i.e., the gas and the dark matter have the same temperatures. In observations, the values of  $\beta$  implied by the density profile fall around 0.6 less than unity. This may, however, be a result inherent in the  $\beta$ -model, because it is normally applied to observed profiles within a radius significantly smaller than the virial radius (see Akahori & Masai 2005). We put  $T(0) = T_0$  for normalization and calculate  $T'(r)/T(0)$  with a boundary condition  $T'(r_{\text{cool}}) = T(r_{\text{cool}})$ . It should be noted that  $T(r_{\text{cool}})/T(0)$  depends on the potential profile and  $\gamma$ , and thus  $T'(r)/T(0)$  does as well, which is not explicitly seen in equation (11), though.

Once the gas inflow takes place and attains to a steady state, and the quasi-hydrostatic condition is achieved, we may have

$$\frac{1}{\rho'} \frac{dP'}{dr} \simeq \frac{1}{\rho} \frac{dP}{dr} \simeq -G \frac{M_{\text{DM}}(r)}{r^2}, \quad (12)$$

where  $\rho'$  and  $P'$  are the gas density and the gas pressure, respectively, of the cool core. The ram pressure is negligible compared to the thermal one in this balance. Thus, for a given  $T'(r)$ , the density profile

$$\frac{d \ln \rho'}{d \ln r} \simeq -\frac{d \ln T'}{d \ln r} + \frac{T}{T'} \gamma \frac{d \ln \rho}{d \ln r} \quad (13)$$

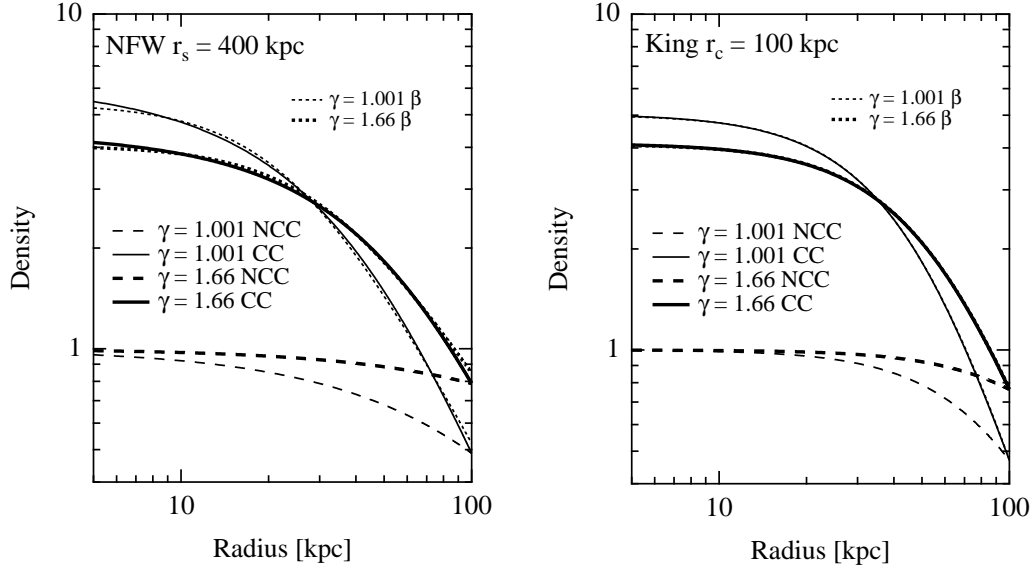
follows; note that  $\gamma$  is defined for  $P$  (or  $T$ ) and  $\rho$ . In the cool core concerned in these calculations,  $T/T'$  varies with the radius from 1 at  $r = r_{\text{cool}}$  to  $\sim 3$  at  $r \sim 0$ , and the gas is kept (quasi-) hydrostatic through the core. Actually, in order that the inflow occurs, the left-hand side must be once larger than the right-hand side in equation (12); note that  $dP/dr$  is negative.

Using equation (13) with  $T(r)$  and  $\rho(r)$  obtained in the last subsection and  $T'(r)$  from equation (11), we calculate  $\rho'(r)/\rho(0)$  with  $\rho'(r_{\text{cool}}) = \rho(r_{\text{cool}})$ , and show it in figure 2 by the solid lines (denoted by CC) for a typical cooling radius of  $r_{\text{cool}} = 100$  kpc (e.g., Peterson & Fabian 2006). The initial-gas density is taken to be a polytropic distribution of  $\gamma = 1.001$  or 1.66 (see subsection 2.1) and represented by the broken line (NCC). The virialized gas of  $\gamma \simeq 1$  polytrope may be attained, e.g., if in the history of the cluster formation merger shocks are radiative or thermal conduction works in the core. Note that the quasi-hydrostatic cooling (Masai & Kitayama 2004) predicts a steeper profile than the hydrostatic one of  $\gamma = 1.001$  polytrope.

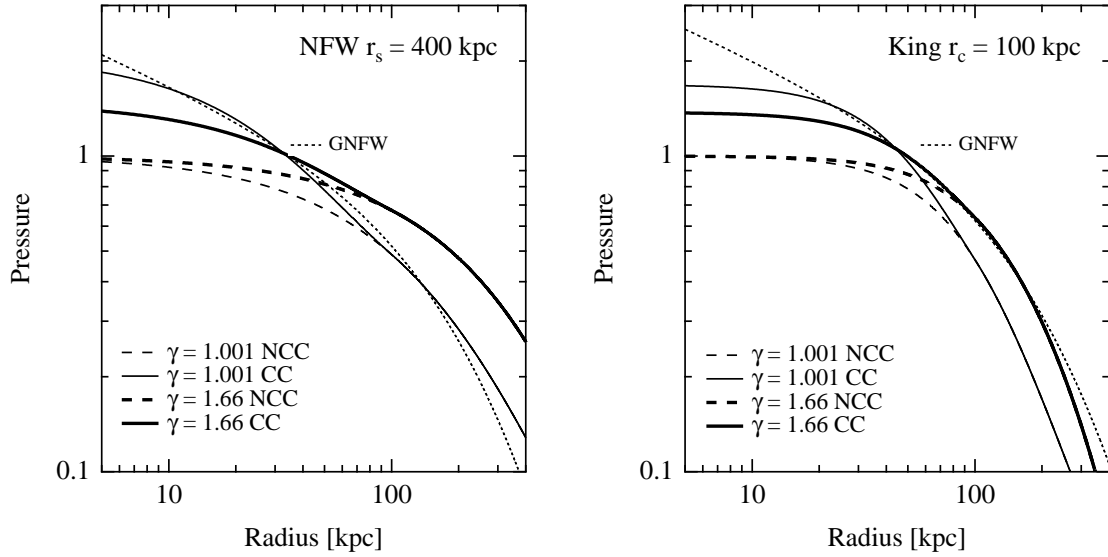
In figure 2, the dotted lines (denoted by  $\beta$ ) represent the best-fit  $\beta$ -model,  $n(r) = n_0 [1 + (r/r_{\text{c,gas}})^2]^{-3\beta/2}$  with  $n$  and  $r_{\text{c,gas}}$  being the density and the core radius of gas, to imitate the density of CC at  $5 < r/\text{kpc} < 100$ . These parameters are given in table 1, where is also shown the parameters for the initial noncool cores in the range  $5 < r/\text{kpc} < 400$ . At  $r < r_{\text{cool}}$  the  $\beta$ -model can reproduce the density of CC fairly well for the NFW potential and quite well for the King one; systematically, the  $\beta$ -model gives a flatter profile toward the center than the calculation for the NFW. This result may suggest that analysis by the  $\beta$ -model is also useful for cool cores if the gas is quasi-hydrostatic, though not relevant to its original meaning.

Figure 3 shows the pressure profile,  $\rho(r)T(r)/[\rho(0)T(0)]$  (broken lines, NCC) and  $\rho'(r)T'(r)/[\rho(0)T(0)]$  (solid lines, CC). It can be seen that in the quasi-hydrostatic cooling core ( $r \lesssim r_{\text{cool}} = 100$  kpc) the pressure profile for the initially isothermal ( $\gamma = 1.001$ ) gas is steeper than that for the  $\gamma = 1.66$  gas, and the profile in the inner core for the NFW potential than that for the King one. The best-fit generalized NFW (GNFW, hereafter; Nagai et al. 2007) pressure obtained for the REXCESS sample of clusters (Arnaud et al. 2010 Eqs. 11–12),  $p(x) = P_0(c_{500}x)^{-\theta} [1 + (c_{500}x)^\zeta]^{-(\eta-\theta)/\zeta}$  for  $(P_0, c_{500}, \theta, \zeta, \eta) = (8.403h_{70}^{-3/2}, 1.177, 0.3081, 1.0510, 5.4905)$ . The GNFW profile is normalized so as to pass the intersection of  $\gamma = 1.001$  and  $\gamma = 1.66$  curves of quasi-hydrostatic cooling gas (CC).

Figures 4 shows the entropy profile,  $T(r)/\rho^{2/3}(r)/[T(0)/\rho^{2/3}(0)]$  (broken lines, NCC) and



**Fig. 2.** Gas-density profile of quasi-hydrostatic cool cores,  $\rho'(r)/\rho(0)$  (solid lines, CC) with  $r_{\text{cool}} = 100$  kpc and the initial noncool ones,  $\rho(r)/\rho(0)$  (broken lines, NCC) of  $\gamma = 1.66$  (thick lines) or 1.001 (thin lines) polytrope. The dotted lines represent the best-fit  $\beta$ -models (see text). Particularly in the right panel, the best-fit  $\beta$ -models (thin- and thick-dotted lines) reproduce the calculated CC density profiles (thin- and thick-solid lines) well and almost perfectly overlap with them for both  $\gamma = 1.001$  and 1.66, respectively.



**Fig. 3.** Gas-pressure profile of quasi-hydrostatic cool cores,  $\rho'(r)T'(r)/[\rho(0)T(0)]$  (solid lines, CC) with  $r_{\text{cool}} = 100$  kpc and the initial noncool ones,  $\rho(r)T(r)/[\rho(0)T(0)]$  (broken lines, NCC) of  $\gamma = 1.66$  (thick lines) or 1.001 (thin lines) polytrope. The dotted lines represent the GFW-pressure profile obtained for REXCESS sample by Arnaud et al. (2010) (see text).

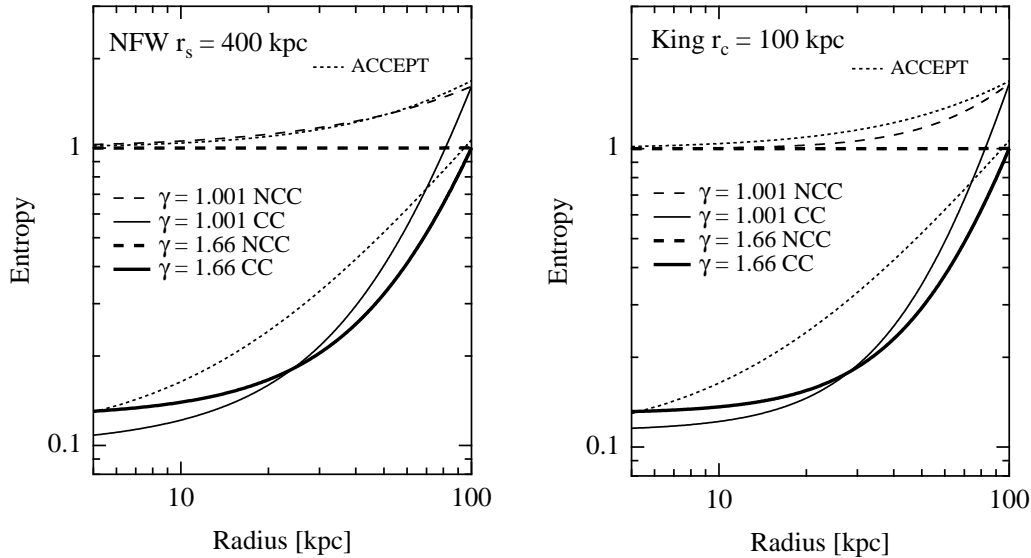


**Fig. 4.** Entropy profile of quasi-hydrostatic cool cores,  $T'(r)/\rho^{2/3}(r)/[T(0)/\rho^{2/3}(0)]$  (solid lines, CC) with  $r_{\text{cool}} = 100$  kpc and the initial noncool ones,  $T(r)/\rho^{2/3}(r)/[T(0)/\rho^{2/3}(0)]$  (broken lines, NCC) of  $\gamma = 1.66$  (thick lines) or  $1.001$  (thin lines) polytrope. The upper- and lower-dotted curves in each panel indicate the best-fit entropy profiles to the ACCEPT sample with high ( $K_0 > 50$  keV cm $^2$ ) and low ( $K_0 \leq 50$  keV cm $^2$ ) central entropy values (Cavagnolo et al. 2009), respectively.

**Table 1.**  $\beta$ -model parameters for density profiles of non-cool and cool cores.

Potential		$\gamma = 1.001$			$\gamma = 1.66$		
		$n_0^*$	$r_{\text{c,gas}}$ [kpc]	$\beta$	$n_0$	$r_{\text{c,gas}}$ [kpc]	$\beta$
NFW	NCC	0.89 (1.00)	64	0.33	0.95 (1.00)	104	0.25
NFW	CC	5.41 (6.24)	25	0.55	4.05 (4.43)	33	0.45
King	NCC	1.00 (1.00)	100	0.53	0.99 (1.00)	164	0.44
King	CC	5.02 (5.05)	51	1.0	4.10 (4.13)	58	0.81

\* Central density normalized by that for the non-cool core. The value in parenthesis denotes the central surface brightness obtained from the present calculation.

$T'(r)/\rho^{2/3}(r)/[T(0)/\rho^{2/3}(0)]$  (solid lines, CC). While the initial polytropic gas (NCC) exhibits a flat or shallower profile, the cooling gas (CC) exhibits entropy roughly  $\propto r$  at  $0.1 < r/r_{\text{cool}} < 1$  for both the NFW and King potentials. The best-fit profiles obtained by Cavagnolo et al. (2009) for the ACCEPT cluster sample are also shown by the dotted lines, so that their high central entropy  $K_0$  ( $> 50$  keV cm $^2$ ) is unity at  $r = 0$ . Note that their entropy profile consists of a power-law and a constant,  $K(r) = K_0 + K_{100}(r/100 \text{ kpc})^\alpha$ , and the best-fit parameters for clusters with  $K_0 \leq 50$  and  $K_0 > 50$  keV cm $^2$  are  $(K_0, K_{100}, \alpha) = (16.1, 150, 1.20)$  and  $(156, 107, 1.23)$ , respectively.

Comparisons between the calculated density, pressure, and entropy and their observations are discussed in the next section. It should be noted here that  $r_{\text{cool}}$  is a point at which the temperature, and thus quantities derived therefrom, are not smoothly connected to those on the outside, since we consider the cooling within  $r_{\text{cool}}$  while leaving the initial polytropic value as it is outside.

The picture discussed in this section is valid as long as the sound crossing time is sufficiently shorter than  $\tau_{\text{cool}}$ .

In other words, without any heating process, the sound speed decreases with the cooling, and eventually ceases to readjust the pressure against the gravitational force. A flattening of  $\rho'(r)$  toward the center is due to a (quasi-) hydrostatic balance, and the actual  $\rho'(r)$  could be steeper in hydrodynamics. Note that  $T'$  or  $\rho'$  here is not applicable to the deep core in which the gas accumulates, and also recall that we ignore the gas mass in comparison to the gravitational potential. In the quasi-hydrostatic cooling phase, equation (12) or (13) can be a good approximation of typical cool cores. The results presented here are useful for the  $\beta$ -model based or such a hydrostatic-balance based analysis, as discussed in the following section.

### 3. Discussion

#### 3.1. Comparison with Observed Core Radii and Density profiles

As can be seen in figure 2 or table 1, the core radius in the quasi-hydrostatic cooling phase is about one-third of the initial radius of polytropic gas in the virial equilibrium. If clusters that are relaxed or virialized but not yet



cooling-affected, have  $\sim 200$  kpc cores, the clusters at the quasi-hydrostatic cooling stage appear to have  $\sim 60$  kpc cores. This result is consistent with the hydrodynamical calculation by Akahori & Masai (2006), who analyzed the calculated clusters using the  $\beta$ -model.

In figure 5, the gas-density profiles are compared with the best-fit  $\beta$ -model profiles for clusters analyzed in Ota et al. (2006). Note that the systematic error of the central-gas density derived under the isothermal  $\beta$ -model is estimated to be small (the Appendix), which does not affect the present discussion. In figure 5, the solid (CC) and broken (NCC) black lines represent the density  $\rho'$  of the quasi-hydrostatic cool core and  $\rho$  of the initial polytropic noncool core, respectively. These calculated-density profiles are normalized such that the cooling time at  $r_{\text{cool}}$  is equal to 10 Gyr in the figure.<sup>1</sup>

One can see that the initial density,  $\rho$  (broken lines), falls around the upper bounds of the densities of larger-core ( $r_c > 100$  kpc) clusters, most likely relaxed, but not yet cool-core clusters. The density  $\rho'$  (solid lines) of the quasi-hydrostatic cool core, on the other hand, lies between the mid- and high-values of the densities of small-core ( $r_c < 100$  kpc) clusters. We also found from the literature on the spatially resolved X-ray spectroscopy of clusters (Allen et al. 2001; Bonamente et al. 2006; Zhang et al. 2007; Zhang et al. 2008; Snowden et al. 2008) that 11 small-core clusters out of 13 plotted in figure 5 have a clear decrease in temperature at the center, while none of 17 large-core clusters has such a temperature drop.

The above facts may support that the density increase in the cool core can be accounted for by the quasi-hydrostatic cooling, and that our calculation gives a typical density of cool cores. However, there exists a large scatter, and some observed clusters have higher central densities than predicted ones. In the context concerned here, the scatter is ascribed to that in the potential profile and/or to those in the initial-inflow condition and the elapsed time.

### 3.2. Comparison with Observed Pressure and Entropy Profiles

Arnaud et al. (2010) discussed a universal-pressure profile for the REXCESS cluster sample, and obtained the best-fit profile [their equations 11–12] based on GNFW by Nagai et al. (2007). It can be seen from figure 3 that the best-fit GNFW profile is close to the overall ( $10 \lesssim r/\text{kpc} \lesssim 200$ ) slope of quasi-hydrostatic cooling gas of initially  $\gamma = 1.001$  polytrope under the NFW potential. When compared with the GNFW, a depression in the mid-part could arise from non smooth connection in  $\rho'$  and  $T'$  across  $r_{\text{cool}}$  (see subsection 2.2). On the other hand, the difference at  $\gtrsim 200$  kpc is likely due to a difference in the dark-matter potential or  $r_s$ , or to that the cluster gas is not simply hydrostatic. In all cases of  $\gamma$ , it is unlikely that the hydrostatic gas like the initial polytrope here (NCC),

can account for a steep profile in the inner core such as the GNFW.

Cavagnolo et al. (2009) derived radial entropy profiles of ICM for 239 clusters from the *Chandra* data (the ACCEPT sample) to find that the model consisting of a power-law plus a constant  $K(r) = K_0 + K_{100}(r/100 \text{ kpc})^\alpha$  is well fitted to most entropy profiles (see also subsection 2.2). They also showed that the distribution of central entropy  $K_0$  is bimodal, which peaks at  $K_0 \sim 15$  and  $\sim 150 \text{ keV cm}^2$ . Comparing the calculated entropy lines with the best-fit models to the ACCEPT sample (figure 4), we find that the model for clusters with the higher central entropy ( $K_0 > 50 \text{ keV cm}^2$ ) is close to the initial entropy profile for  $\gamma = 1.001$ . As for  $K_0 \leq 50 \text{ keV cm}^2$ , the model is reasonably in agreement with the CC cases in the central decrement, which is lower than that of the initial NCC profiles by about an order of magnitude.

Moreover, for the relation between the scaled temperature and the density, Arnaud et al. (2010) found that the two deviations from their average scaled profiles in the core,  $r/R_{500} < 0.2$ , negatively correlate with each other (figure 3 in their paper); the negative correlation is more clearly seen for cool-core clusters. This behavior is in favor of a quasi-hydrostatic cooling picture.

### 3.3. Beta-model Fit to Surface Brightness Profiles: Physical Basis of Applying Double $\beta$ -Model to Cool Core Clusters

The density profile of the quasi-hydrostatic cool core can be imitated by the  $\beta$ -model with a core radius smaller than that of the initial noncool core, as demonstrated in figure 2. This suggests that either  $\beta$ -model or double  $\beta$ -model can be still fitted to a cool-core cluster, depending also on the available range of radius. Observationally, the double  $\beta$ -model is frequently used to be fitted to the X-ray data of clusters having compact cores or cool cores (e.g., Ota & Mitsuda 2004; Santos et al. 2010). In this subsection, we examine whether the conventional single-component or two-component  $\beta$ -models can be fitted to the X-ray surface brightness expected under quasi-hydrostatic cooling.

We calculated the surface brightness of free-free emission ( $\propto \rho'^2 T^{1/2}$  or  $\propto \rho^2 T^{1/2}$  of cool or noncool core). As can readily be seen in figure 6, the gas core appears smaller in the quasi-hydrostatic cool core than the initial noncool one. We performed the  $\beta$ -model fitting to the calculated surface brightness profiles with the form  $S(r) = S_0[1 + (r/r_{\text{fit}})^2]^{-3\beta+1/2}$ . A radial range of  $5 < r/\text{kpc} < 400$  was used. The best-fit parameters are given in table 2. The surface brightness is enhanced by a factor of 2.4–6.5, and the core radius becomes smaller by a factor of  $\sim 2.5$ –10 for the quasi-hydrostatic cool core in comparison with the initial noncool core. In the lower panels of figure 6, the ratio of the calculated surface brightness profiles to the best-fit  $\beta$ -models are shown. The single-component  $\beta$ -model is reasonably well fitted to the NCC case, while it leaves a systematic deviation from that of the CC case. The chi-squared value, defined as  $\chi^2 \equiv \sum [I(r) - S(r)]^2$ , is also given in table 2. Here,  $I(r)$  represents the calculated

<sup>1</sup> The temperature at the cooling radius is assumed to be  $kT(r_{\text{cool}}) = kT'(r_{\text{cool}}) = 5 \text{ keV}$  in the calculation of cooling time, whose dependence on  $kT$  is, however, so small that it does not affect the present discussion.

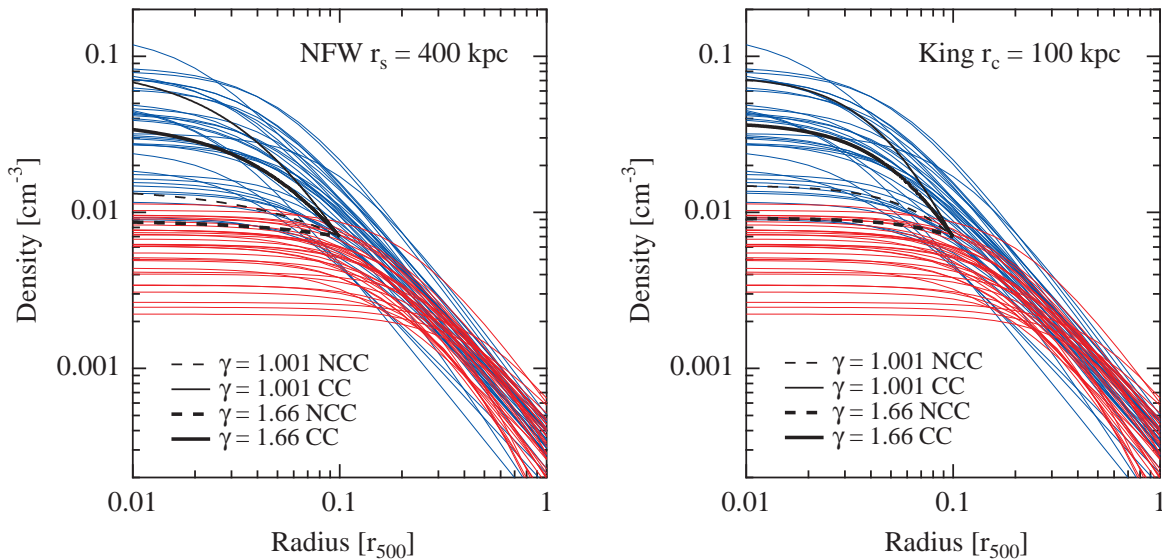


**Fig. 5.** Comparison of calculated gas density profiles with observations. The solid and broken black lines represent the density profiles of quasi-hydrostatic cool cores (CC) and the initial non-cool cores (NCC), respectively, for the NFW (left) and King (right) potential. The calculated density profiles are normalized such that the cooling time at  $r_{\text{cool}}$  is equal to 10 Gyr. The blue and red lines show the electron density profiles of clusters with small ( $r_c < 100$  kpc) and large ( $> 100$  kpc) core radii, respectively (taken from the  $\beta$ -model analysis in Ota et al. 2006.)

surface brightness profile and  $\sum$  sums up all data points.

Next, the double  $\beta$ -model,  $S(r) = \sum_{i=1}^2 S_{0,i} [1 + (r/r_{\text{fit},i})^2]^{-3\beta_i+1/2}$ , is applied to the CC profiles. In this fitting, the inner and outer slope parameters are tied (i.e.,  $\beta_1 = \beta_2$ ) because of a large uncertainty of the inner slope, and capable of varying within 0–2. The two core radii,  $r_{\text{fit},1}$  and  $r_{\text{fit},2}$ , are restricted to a range of 5–400 kpc. As can be seen from figure 7, the surface brightness profile of clusters under radiative cooling can be well approximated by this two-component model. In fact, the systematic deviation in the single  $\beta$ -model fitting is significantly reduced, and the  $\chi^2$  values become smaller in this case (table 2).

The above result gives a physical basis for the use of the double  $\beta$ -model in analyses of the X-ray surface brightness of cool-core clusters. We should note that the resulting  $r_{\text{fit},1}$  or  $r_{\text{fit},2}$  in this analysis is not necessarily equal to the core radius assumed for the potential distribution,  $r_c$ , or that expected through the relationship  $r_c \sim 0.22r_s$  (Makino et al. 1998).

The inner component with a small core size of  $r_{\text{fit},1} \sim 20 - 70$  kpc (table 2) can be ascribed to radiatively cooling gas at the center. The present result will also explain the fiducial emission measure profile obtained by Arnaud et al. (2002) as well as the double-peaked core-size distribution discovered by Ota & Mitsuda (2002); Ota & Mitsuda (2004), whose peak values are  $r_c = 50$  kpc and 200 kpc.<sup>2</sup>

<sup>2</sup> Later, a similar distribution has been shown independently by Hudson et al. (2010) using the high-resolution *Chandra* data on a nearby flux-limited sample. Notice that the detailed statistics of the cool-core formation seems to admit further investigation

### 3.4. Implication on the Time Scale of ICM Thermal Evolution

The fraction of cool-core clusters will give another important clue to understand the formation of cool cores, since it should reflect any time scale relevant to their evolution.

Akahori & Masai (2006) calculated the probability distribution by estimating the time during which a cluster would have a certain core size, to confirm the double-peaked nature of core radius. They suggest that the gas rapidly cools after the quasi-hydrostatic condition breaks. In other words, relaxed clusters with small-core radii currently observed are more or less those at the quasi-hydrostatic cooling stage, which terminates at  $\sim \tau_{\text{cool}}$ . Since  $\tau_{\text{cool}}$  is estimated to be smaller than the Hubble time  $H_0^{-1} \sim 10$  Gyr for a typical cluster, some heating is needed to sustain the system; otherwise, it would be unseen in  $\sim$  Gyr after being virialized. Practically, however, heating due to mergers is likely invoked in cluster evolution, as also suggested from a point of view of radio halos (e.g., Rossetti et al. 2010). The clusters of core radii  $> 400$  kpc in the core-size distribution are possibly attributed to mergers due to their morphology; it should be noted that quasi-hydrostatic cooling is a picture for a relaxed gravitational system. Also other heating/pressure sources, e.g., by black-hole activity, may work. In fact, many “cooling flow” clusters have central cD galaxies hosting black holes. Radio minihalos observed in these clusters may suggest a considerable contribution of the

(e.g., Eckert et al. 2011 and references therein), which is, however, beyond the scope of the present paper.

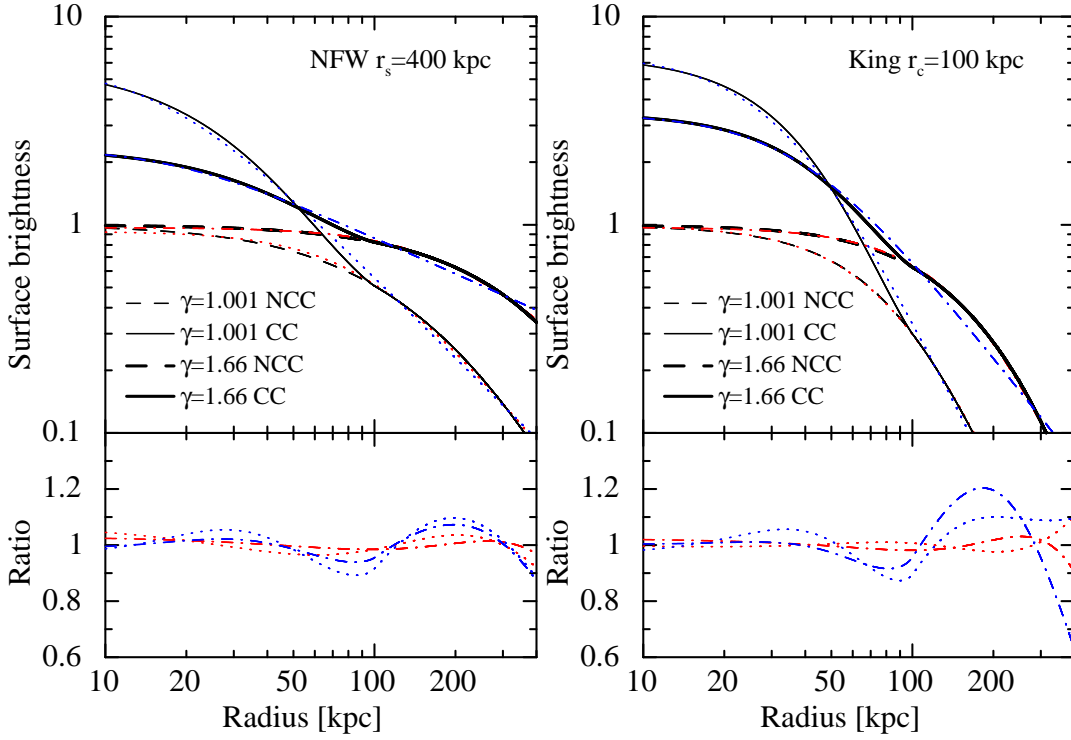


**Fig. 6.** Surface brightness of free-free emission calculated for quasi-hydrostatic cool cores (solid lines, CC) and the initial noncool cores (broken lines, NCC). In the upper panels, the best-fit single  $\beta$ -model are also indicated by the red/blue dotted curves for the NCC/CC cases with  $\gamma = 1.001$  and the red/blue dash-dotted curves for the NCC/CC cases with  $\gamma = 1.66$ , respectively. In the lower panels, the ratios of the calculated surface brightness profiles to the best-fit models are plotted.

**Table 2.**  $\beta$ -model parameters for surface brightness profiles in the noncool and cool cores.

Potential	$\gamma$	Model	$S_{0,1}^*$	$r_{\text{fit},1}$ [kpc]	$\beta_1$	$S_{0,2}^*$	$r_{\text{fit},2}$ [kpc]	$\beta_2$	$\chi^2$	
NFW	1.001	NCC	single- $\beta$	0.93 (1.00)	96	0.44	–	–	1.29	
NFW	1.001	CC	single- $\beta$	5.86 (5.98)	16	0.38	–	–	7.13	
NFW	1.001	CC	double- $\beta$	5.14	28	0.58	0.41	237	0.58	1.61
NFW	1.66	NCC	single- $\beta$	0.97 (1.00)	191	0.37	–	–	–	0.41
NFW	1.66	CC	single- $\beta$	2.34 (2.36)	18	0.26	–	–	–	6.57
NFW	1.66	CC	double- $\beta$	1.52	38	0.57	0.78	400	0.57	0.40
King	1.001	NCC	single- $\beta$	0.99 (1.00)	93	0.69	–	–	–	0.10
King	1.001	CC	single- $\beta$	6.64 (6.54)	35	0.61	–	–	–	5.57
King	1.001	CC	double- $\beta$	6.19	51	0.94	0.23	223	0.94	0.57
King	1.66	NCC	single- $\beta$	0.97 (1.00)	190	0.75	–	–	–	0.49
King	1.66	CC	single- $\beta$	3.42 (3.48)	39	0.44	–	–	–	17.45
King	1.66	CC	double- $\beta$	2.74	74	1.19	0.69	336	1.19	0.30

\* Central surface brightness normalized by that for the noncool core. The value in parenthesis denotes the central surface brightness obtained from the present calculation.



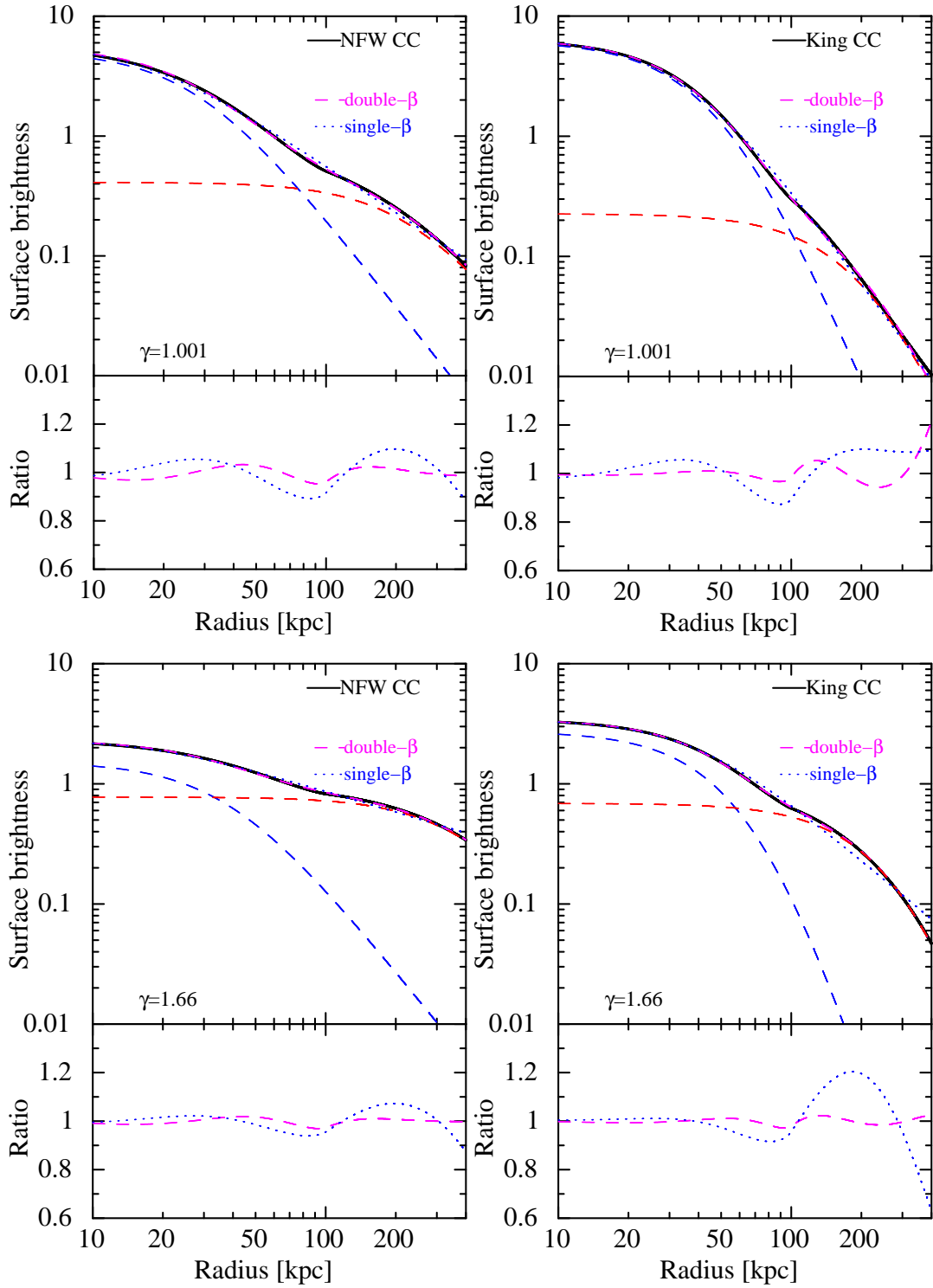


**Fig. 7.** Surface brightness of free-free emission calculated for quasi-hydrostatic cool cores (solid lines, CC). In the upper panels, the best-fit single and double  $\beta$ -models are indicated with the blue dotted and magenta dashed curves. The contributions of two components of the double  $\beta$ -model are also shown with the red and blue curves, respectively. In the lower panels, the ratios of the calculated surface brightness for the cool core to the best-fit single and double  $\beta$ -models are shown with the blue dotted and magenta dashed curves, respectively.

black holes.

Utilizing the technique of the X-ray fundamental plane, Ota et al. (2006) investigated the evolution of X-ray observables for the distant-cluster sample. They showed that the principle axis of the plane is parallel to the  $t_{\text{cool}}$ -axis, suggesting that the cooling time is a parameter to control the core structure. They also noted that the rate of radiative-energy loss is likely to be kept nearly constant for a significant duration of time, even after the onset of cooling in the relaxed systems. This indicates that some steady state is attained for the gas of many small-core clusters. Those results can be consistently understood within the framework of the quasi-hydrostatic model.

Finally, it should be noted that the present calculation shows the evolution of the density profile in the cluster core when the initial NCC profile is given by  $\rho(r)/\rho(0)$  in subsection 2.1; a different initial condition may result in a different CC profile. We ignore the mass of inflow gas through our calculation. At the very late stage of quasi-hydrostatic cooling, however, the inflow gas could alter the gravitational potential in the inner-core region to a steeper profile from the initial equilibrium one. This would break the quasi-hydrostatic condition, and eventually lead to global cooling flow, unless some counter pressure works against, e.g., by heating the gas. Further investigation is needed to obtain a complete view on the thermal evolution of cluster core, including the possibility of heat input due to mergers, as mentioned above.

#### 4. Summary

1. We have calculated the density profile of cool core of intracluster gas in the quasi-hydrostatic cooling phase (Masai & Kitayama 2004), while assuming that the gas is initially in the virial equilibrium state within the dark-matter potential represented by the NFW or King distribution, and has a polytropic profile with  $\gamma = 1.001$  or  $1.66$ .
2. In the quasi-hydrostatic cooling phase, the gas density increases by a factor of 4–6 at the cluster center, while the temperature decreases to about one-third compared with their initial polytropic profiles (noncool core, NCC). Accordingly, the core radius of the cool core (CC) cluster appears to be more compact than the initial polytropic one. This result is consistent with the hydrodynamical simulations by Akahori & Masai (2006).
3. Compared with X-ray observations, it is found that the density profile of CC falls between the mid- and high-values of a small-core ( $r_c < 100$  kpc) when normalized so that the initial-density profile has a cooling time equal to 10 Gyr at the cooling radius.
4. The pressure and entropy profiles are derived for the quasi-hydrostatic cooling gas, and their CC/NCC profiles are compared with the generalized NFW pressure profile for the REXCESS cluster sample (Arnaud et al. 2010) and the best-fit entropy profile models to the ACCEPT sample (Cavagnolo et al. 2009), respectively.
5. The X-ray brightness profiles are calculated for clusters having either the NFW or King potential, while assuming free–free emission. The resulting CC profiles are found to be well represented by the conventional double  $\beta$ -model including the central emission with a compact-core size. This gives a physical basis of applying the double  $\beta$ -model to observed CC clusters. The inner component of the double  $\beta$ -model, which can be ascribed to the radiatively cooling gas at the center, will also explain the fiducial emission measure profiles (Arnaud et al. 2002) as well as the double-peaked core-size distribution (Ota & Mitsuda 2002; Ota & Mitsuda 2004).
6. The implication on the time scale of ICM thermal evolution is discussed. Since the quasi-hydrostatic stage will terminate at  $\tau_{\text{cool}} \sim \text{Gyr} < H_0^{-1}$  for a typical cluster, some heating is needed to sustain the system. The mass of inflow gas is ignored in the present calculation; however, it would alter the the potential distribution of the inner core to an even steeper one at the late stage of cooling, which would break the quasi-hydrostatic balance and lead to global-cooling flow. Further investigation is needed to construct a total view concerning the thermal evolution, including the possibility of heat input due to mergers.

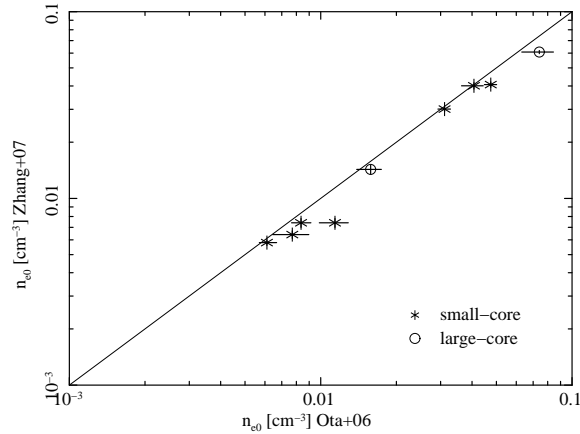
This work was supported in part by a Grant-in-Aid for Young Scientists by MEXT, No. 22740124 (NO) and by a Grant-in-Aid for Scientific Research 18540241 from JSPS (KM).

#### Appendix. Systematic Error of Central Gas Density

Ota et al. (2006) derived the electron density by an isothermal  $\beta$ -model fitting to the surface-brightness profiles. Since the temperature dependence of the X-ray surface brightness is generally small ( $\propto T^{1/2}$ ), the systematic error of the central gas density coming from the temperature drop at the cluster center is expected to be small. Actually, we made a comparison of the central gas density obtained from the *XMM-Newton* observations, having improved resolutions (Zhang et al. 2007), and confirmed that the two samples are in agreement, as shown in figure 8. The figure includes 7 cool-core clusters as well as 2 noncool-core clusters. Thus, the evolution of gas-density profile can be further inferred by comparing the gas densities calculated for the cool and noncool cores in the present work with the  $\beta$ -model profiles presented in Ota et al. (2006).

#### References

- Akahori, T., & Masai, K. 2005, PASJ, 57, 419  
 Akahori, T., & Masai, K. 2006, PASJ, 58, 521  
 Allen, S. W., Schmidt, R. W., & Fabian, A. C. 2001, MNRAS, 328, L37  
 Arnaud, M., Aghanim, N., & Neumann, D. M. 2002, A&A, 389, 1



Zhang, Y.-Y., Finoguenov, A., Böhringer, H., et al. 2008, A&A, 482, 451

**Fig. 8.** Comparison of central gas density between two different samples, Ota et al. (2006) and Zhang et al. (2007). The small- and large-core clusters are denoted by the asterisks and circles, respectively

- Arnaud, M., Pratt, G. W., Piffaretti, R., Böhringer, H., Croston, J. H., & Pointecouteau, E. 2010, A&A, 517, A92
- Bulbul, G. E., Hasler, N., Bonamente, M., & Joy, M. 2010, ApJ, 720, 1038
- Bonamente, M., Joy, M. K., LaRoque, S. J., et al. 2006, ApJ, 647, 25
- Cavagnolo, K. W., Donahue, M., Voit, G. M., & Sun, M. 2009, ApJS, 182, 12
- Chen, Y., Reiprich, T. H., Böhringer, H., Ikebe, Y., & Zhang, Y.-Y. 2007, A&A, 466, 805
- Eckert, D., Molendi, S., & Paltani, S. 2011, A&A, 526, A79
- Fabian, A. C. 1994, ARA&A, 32, 277
- Hudson, D. S., Mittal, R., Reiprich, T. H., Nulsen, P. E. J., Andernach, H., & Sarazin, C. L. 2010, A&A, 513, A37
- Jones, C., & Forman, W. 1984, ApJ, 276, 38
- Makino, N., Sasaki, S., & Suto, Y. 1998, ApJ, 497, 555
- Masai, K., & Kitayama, T. 2004, A&A, 421, 815
- Nagai, D., Kravtsov, A. V., & Vikhlinin, A. 2007, ApJ, 668, 1
- Navarro, J. F., Frenk, C. S., & White, S. D. M. 1997, ApJ, 490, 493
- Neumann, D. M., & Arnaud, M. 1999, A&A, 348, 711
- O'Hara, T. B., Mohr, J. J., Bialek, J. J., & Evrard, A. E. 2006, ApJ, 639, 64
- Ota, N., & Mitsuda, K. 2002, ApJ, 567, L23
- Ota, N., & Mitsuda, K. 2004, A&A, 428, 757
- Ota, N., Kitayama, T., Masai, K., & Mitsuda, K. 2006, ApJ, 640, 673
- Peterson, J. R., & Fabian, A. C. 2006, Phys. Rep., 427, 1
- Rossetti, M., Eckert, D., Cavalleri, B. M., Molendi, S., Gastaldello, F. & Ghizzardi, S. 2011, A&A, 532, A123
- Santos, J. S., Rosati, P., Tozzi, P., Böhringer, H., Ettori, S., & Bignamini, A. 2008, A&A, 483, 35
- Santos, J. S., Tozzi, P., Rosati, P., & Böhringer, H. 2010, A&A, 521, A64
- Snowden, S. L., Mushotzky, R. F., Kuntz, K. D., & Davis, D. S. 2008, A&A, 478, 615
- Suto, Y., Sasaki, S., & Makino, N. 1998, ApJ, 509, 544
- Vikhlinin, A., Kravtsov, A., Forman, W., Jones, C., Markevitch, M., Murray, S. S., & Van Speybroeck, L. 2006, ApJ, 640, 691
- Zhang, Y.-Y., Finoguenov, A., Böhringer, H., et al. 2007, A&A, 467, 437